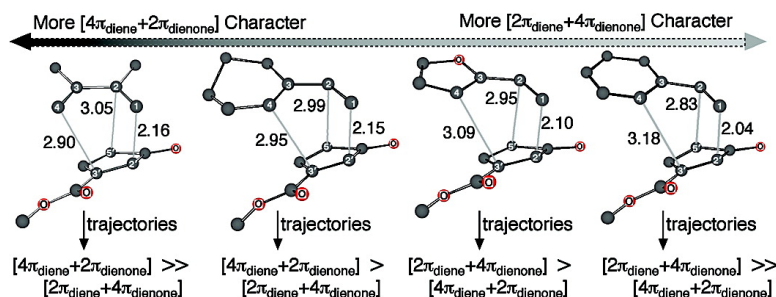Article

Control Elements in Dynamically Determined Selectivity on a Bifurcating Surface

Jacqueline B. Thomas, Jack R. Waas, Michael Harmata, and Daniel A. Singleton

More About This Article

Additional resources and features associated with this article are available within the HTML version:

- Supporting Information
- Access to high resolution figures
- Links to articles and content related to this article
- Copyright permission to reproduce figures and/or text from this article

View the Full Text HTML

Control Elements in Dynamically Determined Selectivity on a Bifurcating Surface

Jacqueline B. Thomas,[†] Jack R. Waas,[§] Michael Harmata,*,[‡] and
Daniel A. Singleton*,[†]

*Department of Chemistry, Texas A&M University, PO Box 30012, College Station, Texas 77842,
Department of Chemistry, University of Missouri - Columbia, Columbia, Missouri 65211, and
Department of Chemistry, Bethel University, St. Paul, Minnesota 55112*

Received April 14, 2008; E-mail: singleton@mail.chem.tamu.edu; harmatam@missouri.edu

Abstract: The mechanism and the nature of the dynamically determined product selectivity in Diels−Alder cycloadditions of 3-methoxycarbonylcyclopentadienone (**2**) with 1,3-dienes was studied by a combination of product studies, experimental kinetic isotope effects, standard theoretical calculations, and quasiclassical trajectory calculations. The low-energy transition structures in these reactions are structurally balanced between $[4\pi_{diene} + 2\pi_{dienone}]$ and the $[2\pi_{diene} + 4\pi_{dienone}]$ modes of cycloaddition. The accuracy of these structures and their bispericyclic nature is supported by the experimental isotope effects. Trajectories passing through these transition structures can lead to both $[4\pi_{diene} + 2\pi_{dienone}]$ and $[2\pi_{diene} + 4\pi_{dienone}]$ cycloadducts, and the mixture of products obtained varies with the structure of the diene. The factors affecting this selectivity are analyzed. The geometry of the transition structure is a useful predictor of the major product, but the selectivity is also guided by the shape of the energy surface as trajectories approach the products and by how trajectories cross the transition state ridge.

1. Introduction

The paradigm of transition state theory is of central importance to the understanding of kinetic selectivity in chemical reactions. Quantitatively, transition state theory allows the selectivity of reactions to be calculated from the energies of competing transition states. Of arguably greater importance, however, is the qualitative role of transition state theory. From the association of rates and selectivities with particular structures, i.e. transition states, the well-known ideas of ground-state structural chemistry provide insight into reactive chemistry. Accordingly, transition states form the ubiquitous, though often implicit, framework for consideration of the nature of experimental selectivities.

Sometimes transition state theory is inapplicable or fails to account for observations. When this happens, analyses must fall back to fundamentals and consider the detailed motions and momenta of atoms, in classical terms their Newtonian dynamics. When unpredictable from transition state theory, the impact of atomic motions and momenta on observations will be referred to here as "dynamic effects."[1] For reactions exhibiting dynamic effects, chemistry must develop new qualitative ideas to account for reactivity and selectivity.

One type of dynamic effect occurs when reactants pass through an initial transition state into a flat area of an energy surface with multiple exit routes to products. The useful qualitative idea in such cases is "dynamic matching," which refers to the tendency to form products that arise from a direct continuation of the trajectories that passed through the initial transition state.[2] Carpenter and others have brought to light the importance of this phenomenon in a series of organic reactions since 1984.[3−6] In a related effect, trajectories can in essence bypass minima on the reaction coordinate.[7,8]

Another type of dynamic effect on selectivity occurs when a reaction involves a "bifurcating energy surface."[9] On such

(2) Carpenter, B. K. *Angew. Chem., Int. Ed.* **1998**, *37*, 3340–3350.

(3) (a) Newman-Evans, R. H.; Carpenter, B. K. *J. Am. Chem. Soc.* **1984**, *106*, 7994–7995. (b) Carpenter, B. K. *J. Am. Chem. Soc.* **1985**, *107*, 5730–5732. (c) Newman-Evans, R. H.; Simon, R. J.; Carpenter, B. K. *J. Org. Chem.* **1990**, *55*, 695–711. (d) Carpenter, B. K. *Acc. Chem. Res.* **1992**, *25*, 520–528. (e) Carpenter, B. K. *J. Am. Chem. Soc.* **1995**, *117*, 6336–6344. (f) Reyes, M. B.; Carpenter, B. K. *J. Am. Chem. Soc.* **2000**, *122*, 10163–10176. (g) Reyes, M. B.; Lobkovsky, E. B.; Carpenter, B. K. *J. Am. Chem. Soc.* **2002**, *124*, 641–651. (h) Nummela, J. A.; Carpenter, B. K. *J. Am. Chem. Soc.* **2002**, *124*, 8512–8513.

(4) (a) Doubleday, C., Jr.; Bolton, K.; Hase, W. L. *J. Am. Chem. Soc.* **1997**, *119*, 5251–5252. (b) Doubleday, C., Jr.; Bolton, K.; Hase, W. L. *J. Phys. Chem. A* **1998**, *102*, 3648–3658. (c) Doubleday, C.; Nendel, M.; Houk, K. N.; Thweatt, D.; Page, M. *J. Am. Chem. Soc.* **1999**, *121*, 4720–4721. (d) Doubleday, C. *J. Phys. Chem. A* **2001**, *105*, 6333–6341. (e) Doubleday, C.; Li, G.; Hase, W. L. *Phys. Chem. Chem. Phys.* **2002**, *4*, 304–312. (f) Doubleday, C.; Suhrada, C. P.; Houk, K. N. *J. Am. Chem. Soc.* **2006**, *128*, 90–94.

(5) Hrovat, D. A.; Fang, S.; Borden, W. T.; Carpenter, B. K. *J. Am. Chem. Soc.* **1997**, *119*, 5253–5254.

(6) (a) Jarzecki, A. A.; Gajewski, J.; Davidson, E. R. *J. Am. Chem. Soc.* **1999**, *121*, 6928–6935. (b) Kless, A.; Nendel, M.; Wilsey, S.; Houk, K. N. *J. Am. Chem. Soc.* **1999**, *121*, 4524–4525.

(7) (a) Carpenter, B. K. *J. Am. Chem. Soc.* **1996**, *118*, 10329–10330. (b) Sun, L.; Song, K.; Hase, W. L. *Science* **2002**, *296*, 875–878.

(8) Debbert, S. L.; Carpenter, B. K.; Hrovat, D. A.; Borden, W. T. *J. Am. Chem. Soc.* **2002**, *124*, 7896–7897.

(9) Ussing, B. R.; Hang, C.; Singleton, D. A. *J. Am. Chem. Soc.* **2006**, *128*, 7594–7607.

[†] Texas A&M University.
[‡] University of Missouri - Columbia.
[§] Bethel University.
(1) This unavoidable term is regrettably confusing: "dynamics" is often used as a synonym for kinetics, and "dynamic effect" is often used to colorfully describe the consequences of conformational equilibria, particularly in enzymes. The usage here is more Newtonian.
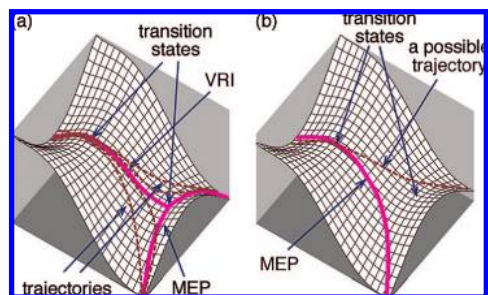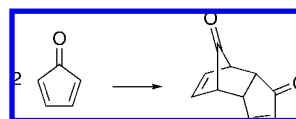
Figure 1. Bifurcating surfaces in which dynamic effects would control selectivity. (a) On a symmetrical surface, the MEP bifurcates at a second transition state. Real trajectories tend to diverge from the MEP in the area of the valley−ridge inflection point (VRI). (b) The surface is unsymmetrical, and the MEP does not bifurcate. However, trajectories may afford a product not on the MEP.
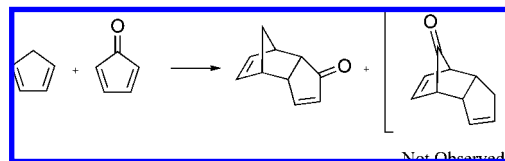
surfaces (Figure 1), reactants that pass through a rate-limiting transition state can proceed to form two products without an additional barrier. For symmetrical surfaces of this type (Figure 1a), the minimum-energy path (MEP) becomes unstable beyond a valley−ridge inflection point (VRI) and ultimately bifurcates at a second transition state, affording two products in equal amounts. Such surfaces are typically associated with symmetry breaking and have been analyzed theoretically for many simple reactions.[10] An organic example of interest here is the dimerization of cyclopentadiene. Theoretical studies by Caramella and co-workers suggest that the cyclopentadiene dimerization involves a C_2-symmetric transition state that is "bispericyclic" and stabilized by two favorable HOMO−LUMO interactions.[11,12] Symmetry breaking after the C_2 transition state affords two identical products.

The related energy surface of Figure 1b, which we will refer to as an "unsymmetrical bifurcating surface" is far less understood, but its consequences are chemically more interesting because trajectories may lead to two nonequivalent products.[7b,13−17] Such surfaces are recognizably similar to the symmetrical

(10) (a) Valtazanos, P.; Ruedenberg, K. *Theor. Chim. Acta* **1986**, *69*, 281–307. (b) Hrovat, D. A.; Borden, W. T. *J. Am. Chem. Soc.* **1992**, *114*, 5879–5881. (c) Wenthold, P. G.; Hrovat, D. A.; Borden, W. T.; Lineberger, W. C. *Science* **1996**, *272*, 1456–1459. (d) Valtazanos, P.; Elbert, S. T.; Ruedenberg, K. *J. Am. Chem. Soc.* **1986**, *108*, 3147–3149. (e) Kraus, W. A.; DePristo, A. E. *Theor. Chim. Acta* **1986**, *69*, 309–322. (f) Windus, T. L.; Gordon, M. S. *Theor. Chim. Acta* **1992**, *83*, 21–30. (g) Windus, T. L.; Gordon, M. S.; Burggraf, L. W.; Davis, L. P. *J. Am. Chem. Soc.* **1991**, *113*, 4356–4357. (h) Yanai, T.; Taketsugu, T.; Hirao, K. *J. Chem. Phys.* **1997**, *107*, 1137–1146. (i) Kumeda, Y.; Taketsugu, T. *J. Chem. Phys.* **2000**, *113*, 477–484. (j) Taketsugu, T.; Kumeda, Y. *J. Chem. Phys.* **2001**, *114*, 6973–6982. (k) Tachibana, A.; Okazaki, I.; Koizumi, M.; Hori, K.; Yamabe, T. *J. Am. Chem. Soc.* **1985**, *107*, 1190–1196. (l) Castaño, O.; Palmeiro, R.; Frutos, L. M.; Luisandrés, J. *J. Comput. Chem.* **2002**, *23*, 732–736. (m) Zhou, C.; Birney, D. M. *Org. Lett.* **2002**, *4*, 3279–3282.
(11) (a) Caramella, P.; Quadrelli, P.; Toma, L. *J. Am. Chem. Soc.* **2002**, *124*, 1130–1131. (b) Quadrelli, P.; Romano, S.; Toma, L.; Caramella, P. *Tetrahedron Lett.* **2002**, *43*, 8785–8789.
(12) Quadrelli, P.; Romano, S.; Toma, L.; Caramella, P. *J. Org. Chem.* **2003**, *68*, 6035–6038.
(13) (a) Yamataka, H.; Aida, M.; Dupuis, M. *Chem. Phys. Lett.* **1999**, *300*, 583–587. (b) Bakken, V.; Danovich, D.; Shaik, S.; Schlegel, H. B. *J. Am. Chem. Soc.* **2001**, *123*, 130–134. (c) Yamataka, H.; Aida, M. *Bull. Chem. Soc. Jpn.* **2002**, *75*, 2555–2569. (d) Mann, D. J.; Hase, W. L. *J. Am. Chem. Soc.* **2002**, *124*, 3208–3209.
(14) Singleton, D. A.; Hang, C.; Szymanski, M. J.; Meyer, M. P.; Leach, A. G.; Kuwata, K. T.; Chen, J. S.; Greer, A.; Foote, C. S.; Houk, K. N. *J. Am. Chem. Soc.* **2003**, *125*, 1319–1328.
(15) Singleton, D. A.; Hang, C.; Szymanski, M. J.; Greenwald, E. E. *J. Am. Chem. Soc.* **2003**, *125*, 1176–1177.
(16) Bekele, T.; Lipton, M. A.; Singleton, D. A.; Christian, C. F. *J. Am. Chem. Soc.* **2005**, *127*, 9216–9223.

Scheme 1

Scheme 2

surfaces because both have adjacent saddle points without an intervening intermediate. However, the MEPs on the unsymmetrical surfaces do not bifurcate. Transition state theory is not able to predict the ratios of products on such surfaces,[18] and presently no qualitative theory exists for predicting the selectivity. Our goal here is to uncover the qualitative control elements of importance to understanding selectivity in a reaction involving an unsymmetrical bifurcating surface.

As will be seen, a unique opportunity to develop an understanding of selectivity on bifurcating surfaces was presented by the cycloadditions of 1,3-dienes with a substituted cyclopentadienone. Cyclopentadienones are extremely reactive in Diels−Alder cycloadditions and readily dimerize in the absence of steric stabilization (Scheme 1).[19] The dimer product is the result of a [4 + 2] cycloaddition, with one molecule acting as the diene and the other as the dienophile.[20] Caramella and co-workers have proposed on the basis of computational studies that the cyclopentadienone dimerization also involves a C_2-symmetric bispericyclic transition state, similar to the cyclopentadiene case previously mentioned, which involves symmetry breaking to afford two identical products.[12] Earlier experimental studies found that when free cyclopentadienone is generated in the presence of a diene, the cyclopentadienone acts exclusively as the dienophile and not as a diene in the observed Diels−Alder product (Scheme 2).[21] However, cyclopentadienone can also act as a reactive diene in Diels−Alder cycloadditions with acetylenic dienophiles.[20] The nature of the periselectivity (selectivity between allowed cycloadditions—here [$4\pi_{diene}$ + $2\pi_{dienone}$] versus [$2\pi_{diene}$ + $4\pi_{dienone}$]—with cyclopentadiene) remains unclear.

Substituted cyclopentadienones are less reactive and have longer lifetimes in solution.[19,22−24] Recently, Harmata has reported numerous examples of periselective Diels−Alder reactions using **1** as a precursor to cyclopentadienone **2** in the

(17) Celebi-Olcum, N.; Ess, D. H.; Aviyente, V.; Houk, K. N. *J. Am. Chem. Soc.* **2007**, *129*, 4528–4529.
(18) For an approach to predicting selectivity on symmetrical bifurcating surfaces, see: Gonzalez-Lafont, A.; Moreno, M.; Lluch, J. M. *J. Am. Chem. Soc.* **2004**, *126*, 13089–13094.
(19) Ogliaruso, M. A.; Romanelli, M. G.; Becker, E. I. *Chem. Rev.* **1965**, *65*, 261–367.
(20) Gaviña, F.; Costero, A. M.; Gil, P.; Palazón, B.; Luis, S. V. *J. Am. Chem. Soc.* **1981**, *103*, 1797–1798.
(21) DePuy, C. H.; Eilers, I. K.; Morris, G. F. *J. Org. Chem.* **1964**, *29*, 3503–3507.
(22) Nantz, M. H.; Fuchs, L. P. *J. Org. Chem.* **1987**, *52*, 5298–5299.
(23) (a) Harmata, M.; Barnes, C. L.; Brackley, J.; Bohnert, G.; Kirchhoefer, P.; Kurti, L; Rashatasakhon, P. *J. Org. Chem.* **2001**, *66*, 5232–5236. (b) Harmata, M.; Pinguan, Z.; Schreiner, P. R.; Navarro-Vázquez, A. *Angew. Chem., Int. Ed.* **2006**, *45*, 1966–1971.
(24) Harmata, M.; Gomez, M. *Eur. J. Org. Chem.* **2006**, *227*, 3–2277.

presence of a base. In the presence of various dienes, the ensuing cycloadditions afford good yields of exclusively *endo cycloadducts* (as defined by the orientation of the cyclopentenone moiety) under mild conditions.[24] The previously obtained products have been the result of solely the [$4\pi_{\text{diene}} + 2\pi_{\text{dienone}}$] mode of cycloaddition on the C2′═C3′ double bond, with no observation of the alternative [$2\pi_{\text{diene}} + 4\pi_{\text{dienone}}$] products. In contrast to the simple situation suggested by the previous results, we expected that the periselectivity of these reactions is in fact decided on a bifurcating energy surface, on the basis of similarity to both theoretical studies of the parent cyclopentadienone reaction and to our experimental studies of cyclopentadiene/ketene reactions.[9] It will be seen that experimental and computational studies support this idea. Mechanistically, these well-behaved reactions with broadly variable dienes provided an excellent opportunity for deeper consideration of the nature of their selectivity.
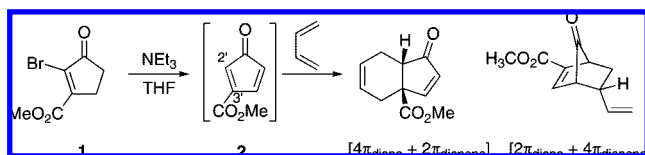
We describe here a mechanistic study of the Diels−Alder cycloaddition of **2** with 1,3-dienes using a combination of product studies, experimental kinetic isotope effects (KIEs), theoretical calculations, and trajectory calculations. The results define the qualitative ideas necessary to understand the dynamically determined selectivity on bifurcating surfaces, including consideration of the detailed transition structure geometry, of how trajectories cross an unsymmetrical transition state ridge, and of the shape of the energy surface as trajectories approach the products.

2. Results

2.1. Continua of Transition States. On the basis of the hypothesis above that the reactions of **2** with 1,3-dienes would involve bifurcating energy surfaces, we sought to examine a range of reactions that varied from preferring [$4\pi_{\text{diene}} + 2\pi_{\text{dienone}}$] periselectivity to preferring [$2\pi_{\text{diene}} + 4\pi_{\text{dienone}}$] periselectivity, with examples exhibiting intermediate selectivity. Toward that end, transition structures for the reaction of **2** with a variety of dienes were surveyed in DFT calculations (see the Supporting Information for examples). From this survey, the reactions of **2** with 2,3-dimethylbutadiene (**3**), 1-vinylcyclohexene (**4**), 2-vinylfuran (**5**), and styrene (**6**) were chosen for further experimental and computational study. Styrene, the extreme example, is not a conventional 1,3-diene, but it can play this role in Diels−Alder reactions.[25]

Transition structures for these reactions were located in MPW1K[26] calculations using a 6-31+G** basis set.[27] These studies were complicated by a diversity of possible modes for the cycloadditions. For example, a total of 16 transition structures were located for the cycloaddition of vinylcyclohexene with **2** in which vinylcyclohexene plays the 4π-component role

in the cycloaddition. These 16 structures arise from the possibility of *endo* versus *exo* orientation of **2** relative to vinylcyclohexene, two possible regiochemical orientations of **2** versus vinylcyclohexene, the possible involvement of the C2′═C3′ versus C4′═C5′ double bonds of **2**, and the possibility for attack on vinylcyclohexene from two faces defined by the half-chair conformation of the cyclohexene ring. (See the Supporting Information for a complete list of the structures located.) Fortunately, the consideration of these reactions was simplified by a strong preference for *endo* transition structures (the *exo* transition structures were at least 4 kcal/mol higher in energy), a strong preference for reaction at C2′═C3′ of **2**, and a strong regioselectivity preference favoring bonding of C1 of the dienes with C2′ of **2**. As a result, the reactions of **3**, **5**, and **6** are predicted to be dominated by the single transition structures **7**, **9**, and **10**, while the reaction of **4** has two low-energy transition structures **8-ax** and **8-eq**. (See the Supporting Information for **8-eq**, which is similar to **8-ax** and is 0.2 kcal/mol higher in energy. We refer to **8-ax** as "axial" and **8-eq** as "equatorial" based upon the initial orientation of C4 bond formation on the incipient cyclohexane chair. The axial structure is slightly favored in keeping with related trends in other additions to cyclohexenes.[28] Each of the transition structures **7**, **8-ax**, **8-eq**, **9**, and **10** are spin-stable.)

The striking feature of these transition structures is that they have qualities of both [$4\pi_{\text{diene}} + 2\pi_{\text{dienone}}$] and [$2\pi_{\text{diene}} + 4\pi_{\text{dienone}}$] cycloadditions. This bispericyclic character,[11,12] likely contributing to the low energy of the structures versus alternatives, can be seen in the similarity of the C4−C3′ and C2−C5′ distances in each structure. Based on the C4−C3′ versus C2−C5′ distances, structure **7** may be described as having greater [$4\pi_{\text{diene}} + 2\pi_{\text{dienone}}$] character while the styrene transition structure **10** is more [$2\pi_{\text{diene}} + 4\pi_{\text{dienone}}$] in character, with **8-ax** and **9** in between. Notably, the [$4\pi_{\text{diene}} + 2\pi_{\text{dienone}}$] versus [$2\pi_{\text{diene}} + 4\pi_{\text{dienone}}$] character of these transition structures seems closely related to the relative stability of the possible products. For **7** and **8-ax**, the [$4\pi_{\text{diene}} + 2\pi_{\text{dienone}}$] products **11** and **13** are more stable by 22.6 and 10.3 kcal/mol, respectively, than the [$2\pi_{\text{diene}} + 4\pi_{\text{dienone}}$] products **12** and **14** (MPW1K/6-31+G** + zpe). For **9** and **10**, the [$2\pi_{\text{diene}} + 4\pi_{\text{dienone}}$] products **15** and **17** are more stable than the [$4\pi_{\text{diene}} + 2\pi_{\text{dienone}}$] products **16** and **18** by 1.5 and 12.8 kcal/mol, respectively.

This intriguing continuum of transition structures is necessarily subdivided in MEP analyses since a steepest-descent path can only lead to a single product. The MEPs (in mass-weighted coordinates) passing through **7** and **8-ax** lead to the [$4\pi_{\text{diene}} + 2\pi_{\text{dienone}}$] products **11** and **13**, while the MEPs passing through **9** and **10** lead to [$2\pi_{\text{diene}} + 4\pi_{\text{dienone}}$] cycloadducts **15** and **17**. It will be seen below that trajectories through these transition structures are not so cleanly subdivided. A search was undertaken for alternative transition state structures that were mainly [$2\pi_{\text{diene}} + 4\pi_{\text{dienone}}$] in character for reactions of **3** and **4** or mainly [$4\pi_{\text{diene}} + 2\pi_{\text{dienone}}$] in character for reactions of **5** and **6**. No low-energy structures of these types could be located. (High-energy examples involving *exo* transition structures were readily located; see the Supporting Information). Instead, attempts to locate transition structures for the alternative cycloaddition modes invariably reconverged on **7**, **8-ax**, **9**, and **10**. This is consistent with a merging of [$4\pi_{\text{diene}} + 2\pi_{\text{dienone}}$] and [$2\pi_{\text{diene}} + 4\pi_{\text{dienone}}$] pathways through the transition

(25) (a) Carreño, M. C.; Urbano, A. *Tetrahedron Lett.* **2000**, *41*, 4117–4121. (b) Manning, W. B. *Tetrahedron Lett.* **1979**, *20*, 1661–1664.

(26) Lynch, B. J.; Fast, P. L.; Harris, M.; Truhlar, D. G. *J. Phys. Chem. A* **2000**, *104*, 4811–4815.

(27) (a) Frisch, M. J.; *Gaussian 03*, Revision C.02; Gaussian, Inc.: Wallingford CT, 2004. (b) See the Supporting Information for full details on the calculational methods employed.

(28) Boren, B; Hirschi, J. S.; Reibenspies, J. H.; Tallant, M. D.; Singleton, D. A.; Sulikowski, G. A. *J. Org. Chem.* **2003**, *68*, 8991–8995.
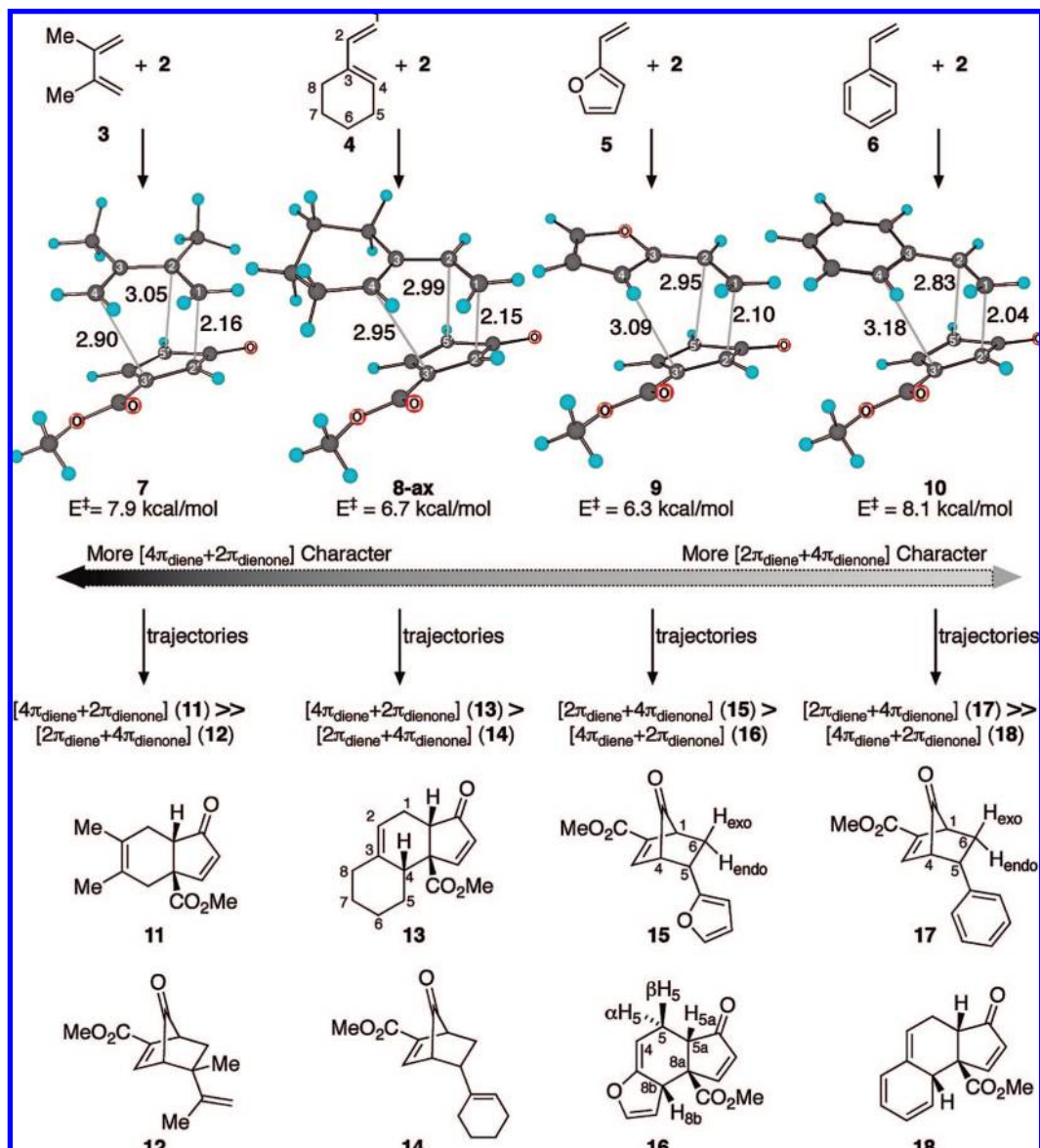
Figure 2. Low-energy cycloaddition transition structures for the reactions of **2** with **3**, **4**, **5**, and **6**, along with a summary of trajectory studies on the transition structures and the structures of the possible products. Activation barriers (MPW1K/6-31+G** + zpe) are versus separate starting materials in kcal/mol.

structures, and supports the involvement of bifurcating energy surfaces qualitatively resembling those of Figure 1.

A second continuum of transition structures is of importance here. As discussed in the introduction, bifurcating energy surfaces are recognizable by the presence of a second geometrically adjacent saddle point without an intervening intermediate. The adjacent saddle points in the systems here are the transition structures for for the [3,3]-sigmatropic (Cope) rearrangements interconverting the $[4\pi_{diene} + 2\pi_{dienone}]$ and $[2\pi_{diene} + 4\pi_{dienone}]$ products. The transition structures located for these rearrangements are shown in Figure 3, and their geometric proximity to the cycloaddition transition structures of Figure 2 is obvious. However, one difference in the trends in the two continua seems important. While the cycloaddition transition structures geometrically favored the more stable product, the rearrangement transition structures, following Hammond's postulate, more closely resemble the less stable product. For example, **7** is geometrically closer to **11** than to **12**, while **19** more closely resembles **12** than **11**. As the relative stabilities

of the products change, the cycloaddition and rearrangement transition structures shift in opposite directions!

2.2. Product Studies. The reaction of **2** with **3** has been previously reported[24] and affords the $[4\pi_{diene} + 2\pi_{dienone}]$ product **11** as the only observable cycloadduct except for traces of materials arising from apparent dimerization of **2**. The reaction of **2** with vinylcyclohexene, also previously reported,[24] affords the single cycloadduct **13**, though it will be seen that this reaction is more complex than it appears. Product **13** is notably the *endo*-isomer that would arise from **8-ax** or **8-eq**, and no traces of either *exo*-adducts or the possible alternative regioisomer were observed. For reasons to be described later, particular care was taken in many attempts to observe the alternative $[2\pi_{diene} + 4\pi_{dienone}]$ product **14** in the reaction mixture, but no evidence for its formation was obtained.

The reaction of 2-vinylfuran (**5**) with **2** was more complicated, affording both the $[2\pi_{diene} + 4\pi_{dienone}]$ product **15** and the $[4\pi_{diene} + 2\pi_{dienone}]$ product **16** as the only mixed cycloadducts in a ratio of 1.6:1 at 25 °C in two days. Product **15** was isolated in
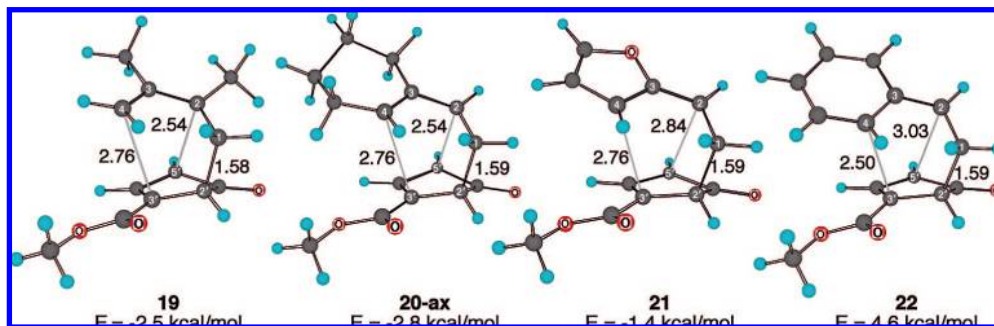
Figure 3. MPW1K/6-31+G** transition structures for the [3,3]-sigmatropic (Cope) rearrangements interconverting the [$4\pi_{diene} + 2\pi_{dienone}$] products **11**, **13**, **16**, and **18** and the [$2\pi_{diene} + 4\pi_{dienone}$] products **12**, **14**, **15**, and **17**. Energies (MPW1K/6-31+G** + zpe) are versus separate **2**/diene, in kcal/mol, to be on the same scale as the energies of Figure 2.

27% yield, while the dearomatized **16** was unstable during chromatographic isolation but could be obtained with ∼80% purity in 19% yield. The stereochemistries of **15** and **16** were assigned from analysis of their ^{1}H NMR coupling constants and COSY spectra. The H_{exo} in **15** was assigned on the basis of a 5.2 Hz coupling constant with the bridgehead hydrogen at C1, while H_{endo} shows no coupling with this hydrogen. The hydrogen at C5 was then assigned as *exo* on the basis of a 9.6 Hz coupling with H_{exo} and a 4.6 Hz coupling with H_{endo}.[29,30] In assigning the stereochemistry of **16**, the observation of relatively small coupling constants to H_{5a} (6.0 and 2.0 Hz) was important. The predicted coupling constants[31] for the *endo*-isomer **16**, based on the lowest-energy conformation in MM3 calculations, were 5.6 Hz for $H_{5a}–\beta H_5$ and 1.4 Hz for $H_{5a}–\alpha H_5$, matching well with the observed values. In the alternative *exo* analogue of **16**, the predicted coupling constants were 10.0 and 7.6 Hz, matching poorly with the observed values.

The formation of **16** is particularly striking since the computational studies were unable to locate any cycloaddition transition structure that leads by a steepest-descent path to **16**. A conventional theoretical study thus cannot predict that **16** will be formed. The formation of **16** from **9** will be explained by trajectory studies.

Styrene is somewhat less reactive with **2** than typical 1,3-dienes are, so that dimerization of **2** becomes competitive. With excess styrene at room temperature, the reaction affords **17** as the only styrene adduct in 36% yield. H_{exo} in **17** was assigned from its 4.0 Hz coupling constant with the bridgehead hydrogen at C1, while H_{endo} was not coupled with this hydrogen. The hydrogen at C5 was assigned as *exo* on the basis of a 9.8 Hz coupling with H_{exo} versus a 6 Hz coupling with H_{endo},[29,30] and this confirms that the phenyl group is *endo*.

2.3. Cope Rearrangements and Kinetic versus Thermodynamic Control. Because the [$4\pi_{diene} + 2\pi_{dienone}$] versus [$2\pi_{diene} + 4\pi_{dienone}$] products in these reactions are potentially interconverted by a Cope rearrangement, we consider here whether the experimental product observations are the result of kinetic or thermodynamic control. In the case of **15** versus **16**, this was readily evaluated experimentally. The ratio of products from the 25 °C reaction was unchanged after 17 days at 25 °C, while

isolated **15** underwent no significant isomerization to **16** in 60 days. The combination of these observations indicates that the observed ratio is kinetically controlled.

In the other reactions, the unobserved alternative products **12**, **14**, and **18** are higher in energy so we were unable to experimentally determine whether the observed products are the result of kinetic control. As will be seen, the issue of kinetic versus thermodynamic control was of particular interest for the vinylcyclohexene system, and we considered carefully whether the issue could be resolved from the computational studies. Transition structure **20-ax** for the interconversion of **13** and **14** was predicted to be 28.9 kcal/mol (MPW1K/6-31+G** + ZPE) above **14**. If this barrier were accurate, the rearrangement of **14** at 25 °C would be quite slow, and based on the trajectory studies below, **14** should have been observable.

However, the MPW1K calculations appear to overestimate the barrier in these reactions. In the related [3,3]-sigmatropic rearrangement of **23**, Zwanenburg observed the slow equilibration of **23** and **24** at 25 °C.[32] If one estimates from their observations that the rate constant for the rearrangement is on the order of 10^{-5} s^{-1}, $\Delta G^{\ddagger}$ would be ∼24 kcal/mol. A transition structure was located for the [3,3]-sigmatropic rearrangement of **23** (see Supporting Information), and the calculated $\Delta G^{\ddagger}$ was 31.0 kcal/mol (MPW1K/6-31+G**, including harmonic thermal energy and entropy estimates). Since MPW1K overestimates this barrier by ∼7 kcal/mol, a similar overestimate of the barrier for the rearrangement of **14** is likely. MP2 single point calculations (MP2/6-31+G**//MPW1K/6-31+G** + ZPE) place the barriers for rearrangement of **14** and **23** at 21.6 and 24.4 kcal/mol, respectively. MP2 tends to underestimate barriers for pericyclic reactions, but if the 2.8 kcal/mol difference in the barrier for **14** versus **23** is correct, **14** would rearrange ∼115 times faster than **23**, and it would be difficult to observe under the reaction conditions.
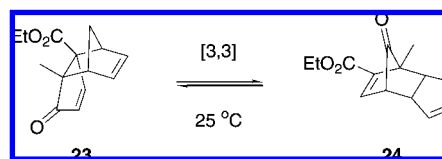
The predicted barrier for rearrangement of **16** is 25.2 kcal/mol (MP2/6-31+G**//MPW1K/6-31+G** + ZPE), in keeping with the observation above of a kinetically controlled product mixture at 25 °C. The situation is less certain with **11/12**, as

(29) Jackman, L. M.; Sternhell, S. *Applications of Nuclear Magnetic Resonance Spectroscopy in Organic Chemistry*; Pergamon Press: Oxford, 1969; pp 280–304.

(30) (a) Laszlo, P.; Schleyer, P; von, R. *J. Am. Chem. Soc.* **1964**, *86*, 1171–1179. (b) Marchand, A. P.; Rose, J. E. *J. Am. Chem. Soc.* **1968**, *90*, 3724–3731.

(31) Haasnoot, C. A. G.; de Leeuw, F. A. A. M.; Altona, C. *Tetrahedron* **1980**, *36*, 2783–2792.

(32) Klunder, A. J. H.; Lange, J. H. M.; Zwanenburg, B. *Tetrahedron Lett.* **1987**, *28*, 3027–3030.
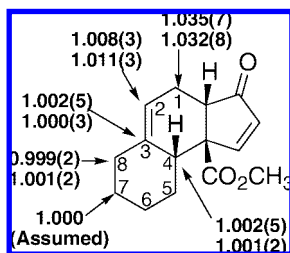
Figure 4. Experimental ^{13}C KIEs (k_{12C}/k_{13C}) for the Diels–Alder reaction of **1** with vinylcyclohexene. KIEs at C5 and C6 were not determined because of the near-overlap of the ^{13}C peaks.

the predicted barrier for rearrangement of **12** is 23.7 kcal/mol, but so little **12** is expected from any prediction (see below) that no effort was made to observe it. The observation of **18** would be very difficult at temperatures conducive to the cycloaddition, as the predicted barrier for its rearrangement is 18.6 kcal/mol, but no **18** is expected from either a conventional computational analysis or the trajectory studies below.

2.4. Experimental Isotope Effects. While synthetic reactions of **1** with vinylcyclohexene mediated by triethylamine have been conducted under refluxing conditions in THF or toluene,[24] the reaction proceeds quite cleanly at room temperature, albeit more slowly, and these conditions were used for the KIE studies here. The ^{13}C KIEs (k_{12C}/k_{13C}) for the vinylcyclohexene component of the cycloaddition were determined combinatorially at natural abundance by NMR methodology.[33] While it is usually advantageous to analyze recovered starting material when determining KIEs in this way,[33a] analysis of the product at low conversion versus 100% conversion[33b,c] was employed here to avoid the need for an excess of **1** in a large-scale reaction. Two reactions were taken to 13% conversion and the product **13** was isolated by extractive workup followed by flash chromatography. The samples were then analyzed by ^{13}C NMR in comparison to a standard sample of **13** obtained from a small-scale reaction taken to 100% conversion. The relative changes in ^{13}C isotopic composition in each position were determined using C7 as an "internal standard" with the assumption that the KIE at C7 is negligible.

The results are shown in Figure 4. A large ^{13}C KIE of ~1.033 is observed at C1. This fits well qualitatively with the expected substantial σ-bond change at the carbon in the cycloaddition transition state. The relatively small ^{13}C KIE at C4 can be interpreted as the result of the cycloaddition proceeding through a highly asynchronous transition state,[34] and the small ^{13}C KIE is reminiscent of those observed in corresponding positions in Lewis acid-catalyzed Diels–Alder reactions.[35] The ^{13}C KIE at C2 is the most difficult to understand, as it is larger than has been observed for the "unreactive" olefinic carbons of the diene in previous studies of carbon KIEs for Diels–Alder reactions.[33a,35,36] The qualitative suggestion from this isotope effect is that some unusual degree of bonding change is occurring at this carbon in the rate-limiting transition state. A more detailed discussion of this isotope effect will be given below.

Table 1. Results from quasiclassical trajectories starting from transition structures **7**, **8-ax**, **8-eq**, **9**, and **10**, and starting from ridge structures **25** and **26**

	$[4\pi_{diene} + 2\pi_{dienone}]$ (formation of **11**, **13**, **16**, or **18**)	$[2\pi_{diene} + 4\pi_{dienone}]$ (formation of **12**, **14**, **15**, or **17**)	recrossing trajectories
Transition Structure			
7	22	2	2
8-ax	28	10	1
8-eq	18	8	1
9	12	19	2
10	0	20	1
Ridge Structure			
25	7	0	7
26	4	7	9

2.5. Trajectory Studies. Because the simplicity of transition state theory cannot be used to theoretically predict the product ratios that should arise on unsymmetrical bifurcating energy surfaces, one must fall back on the detailed consideration of atomic positions and momenta inherent in trajectory studies. Transition structures **7**, **8-ax**, **8-eq**, **9**, and **10** were used as starting points for quasiclassical direct dynamic trajectories[4,5,7,8,37,38] on the MPW1K/6-31+G** potential energy surfaces. Trajectories were initialized with all atomic motions freely variable by giving each normal mode a random sign for its initial velocity, and an initial energy based on a random Boltzmann sampling of vibrational levels appropriate for 298.15 K, including zero-point energy. The mode associated with the imaginary frequency was given a Boltzmann sampling of energy "forward" over the col. The trajectories were propagated employing a Verlet algorithm using 1-fs steps in previously described code[9] and using Gaussian 03[27] to calculate forces at each point until either the $[4\pi_{diene} + 2\pi_{dienone}]$ product (**11**, **13**, **16**, or **18**) or the $[2\pi_{diene} + 4\pi_{dienone}]$ product (**12**, **14**, **15**, or **17**) was formed or recrossing occurred to afford the starting materials. This required 50–100 CPU-hours per trajectory on modern machines. All trajectories were complete within 370 fs and the median times for product formation for **7**, **8** (combined), **9**, and **10** were 70, 109, 129, and 66 fs, respectively. These reaction-coordinate times are short compared to the time scale for collisions with solvent (approximately once per 500–1000 fs) or the time scale of several picoseconds for loss of energy to solvent.[39]

The results are summarized in Table 1. Trajectories started from **7** afforded predominantly the $[4\pi_{diene} + 2\pi_{dienone}]$ product **11**, in keeping with experimental observations and the prediction from the MEP passing through **7**. Trajectories started from **8-ax** or the similar **8-eq** afforded a majority of the observed **13**, but the trajectories results predict that a substantial amount (~25–30%) of the alternative product **14** should also be formed.

(33) (a) Singleton, D. A.; Thomas, A. A. *J. Am. Chem. Soc.* **1995**, *117*, 9357–9358. (b) Frantz, D. E.; Singleton, D. A.; Snyder, J. P. *J. Am. Chem. Soc.* **1997**, *119*, 3385–3386. (c) Singleton, D. A.; Schulmeier, B. E. *J. Am. Chem. Soc.* **1999**, *121*, 9313–9317.
(34) Beno, B. R.; Houk, K. N.; Singleton, D. A. *J. Am. Chem. Soc.* **1996**, *118*, 9984–9985.
(35) Singleton, D. A.; Merrigan, S. R.; Beno, B. R.; Houk, K. N. *Tetrahedron Lett.* **1999**, *40*, 5817–5821.
(36) Singleton, D. A.; Schulmeier, B. E.; Hang, C.; Thomas, A. A.; Leung, S.-W.; Merrigan, S. R *Tetrahedron* **2001**, *57*, 5149–5160.

(37) (a) Vande Linde, S. R.; Hase, W. L. *J. Chem. Phys.* **1990**, *93*, 7962–7980. (b) Cho, Y. J.; Vande Linde, S. R.; Zhu, L.; Hase, W. L. *J. Chem. Phys.* **1992**, *96*, 8275–8287. (c) Hase, W. L. *Science* **1994**, *266*, 998–1002. (d) Wang, H.; Hase, W. L. *J. Am. Chem. Soc.* **1995**, *117*, 9347–9356. (e) Sun, L.; Hase, W. L.; Song, K. *J. Am. Chem. Soc.* **2001**, *123*, 5753–5756. (f) Vande Linde, S. R.; Hase, W. L. *J. Phys. Chem.* **1990**, *94*, 6148–6150. (g) Li, G.; Hase, W. L. *J. Am. Chem. Soc.* **1999**, *121*, 7124–7129. (h) Wang, Y.; Hase, W. L.; Wang, H. *J. Chem. Phys.* **2003**, *118*, 2688–2695. (i) Sun, L.; Chang, E.; Song, K.; Hase, W. L. *Can. J. Chem.* **2004**, *82*, 891–899.
(38) (a) Bunker, D. L. *Methods Comp. Phys.* **1971**, *10*, 287–325. (b) Bunker, D. L. *Acc. Chem. Res.* **1974**, *7*, 195–201. (c) Chapman, S.; Bunker, D. L. *J. Chem. Phys.* **1975**, *62*, 2890–2899. (d) Suzukawa, H. H., Jr.; Wolfsberg, M.; Thompson, D. L. *J. Chem. Phys.* **1978**, *68*, 455–472. (e) Hase, W. L. *J. Phys. Chem.* **1986**, *90*, 365–374.
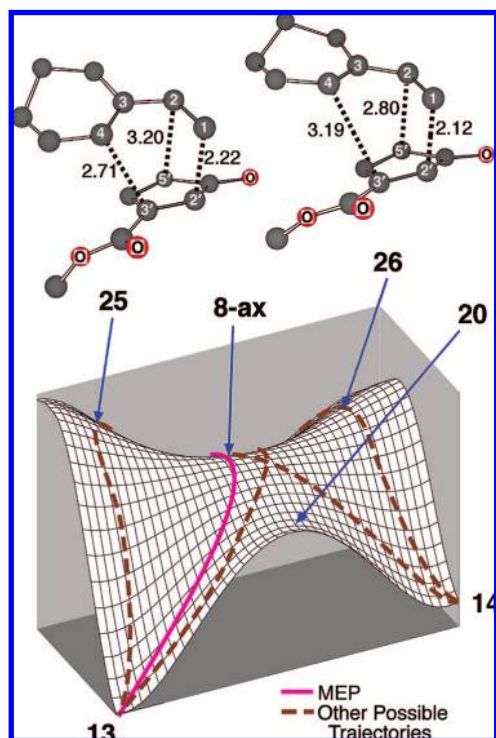(39) Elles, C. G.; Cox, M. J.; Crim, F. F. *J. Chem. Phys.* **2004**, *120*, 6973–6979.

Figure 5. Qualitative energy surface for the reaction of **2** with vinylcyclohexene. Trajectories starting from **2** + vinylcyclohexene (at the back of the surface) could lead to either **13** or **14** through the same transition state area. Due to the anharmonicity or skewed character of the transition state ridge, more trajectories pass to the right of **8-ax**, toward **26**, than to the left, affecting the isotope effects.

As discussed above, isomerization of **14** to **13** can account for **14** not being observed. Trajectories started from **9** preferentially afforded $[2\pi_{diene} + 4\pi_{dienone}]$ product **15** over $[4\pi_{diene} + 2\pi_{dienone}]$ product **16**. The ratio of trajectories forming **15** versus **16**, at 1.58, is strikingly close to experimental observations, though the uncertainty of the predicted ratio based on the necessarily limited number of trajectories is high. All trajectories started from **10** afforded the $[2\pi_{diene} + 4\pi_{dienone}]$ product **17**, in keeping with experimental observations and the prediction from the MEP passing through **10**.

For the purpose here of relating trajectory outcomes to the detailed geometry of the transition structure, the trajectories above were forced through the exact geometries of **7**, **8-ax**, **8-eq**, **9**, and **10**. This has the effect of restricting the phase angles between normal modes to 0 or π. A more realistic model would randomize the phase angles, allowing the trajectories to pass over the transition state "ridge" in a continuum of places, but this would require more trajectories to relate the transition structure geometry to outcome. To examine the effect of randomizing the phase angle, 16 trajectories were carried out using a random linear sampling of displacements along each of the normal modes. Of these, 12 afforded **13** and 4 afforded **14**. This suggests that the restricted sampling for the trajectories in Table 1 does not greatly affect their outcomes.

Figure 5 was constructed to display in more detail the qualitative features of the surface involving **8-ax**. On this surface, the paths for formation of observed product **13** versus alternative product **14** have merged into a broad transition state ridge with **8-ax** as the low point. This ridge may be roughly defined by the displacement of the atoms along a low-energy transverse vibrational normal mode (70 cm^{-1}). This transverse
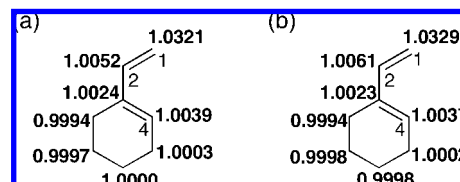

Figure 6. Predicted ^{13}C kinetic isotope effects (k_{12C}/k_{13C}) for the Diels–Alder reaction of **2** with vinylcyclohexene for both (a) **8-ax** and (b) Boltzmann combination of 21 structures based on **8-ax** located along the transition state ridge.

mode is strikingly anharmonic or skewed in character, which will be seen to possibly have experimental consequences.

On a relaxed potential energy surface (fixing C1–C2′, C2–C5′, and C4–C3′ after extension along the 70 cm^{-1} mode), ridge structure **25** is 1.0 kcal/mol above **8-ax**, while ridge structure **26**, displaced equally from **8-ax** in the opposite direction from **25**, is only 0.5 kcal/mol above **8-ax**. The outcome of trajectories should depend on where they cross this ridge, (or more generally, the transition state hypersurface).[40] We hypothesized that trajectories started from **25** would tend to afford **13**, while trajectories started from **26** would tend to afford **14**.

To explore these ideas, structures **25** and **26** were used as starting points for quasiclassical direct dynamic trajectories. The results are summarized in Table 1 and support the hypotheses discussed above. Trajectories from **25** afford exclusively **13**. Trajectories from **26** are more likely to afford **14** than **13**, though it is notable for later discussion that they can still afford **13** despite the bias of structure **26** toward formation of **14**.

2.6. Predicted Isotope Effects. For comparison with the experimental KIEs, KIEs were predicted from the computational studies in two ways. The first way employed conventional transition state theory. The second way, which is novel, allowed for the anharmonicity of the transition state ridge.

The ^{13}C KIEs based on **8-ax** were predicted from scaled theoretical vibrational frequencies[41] using conventional transition state theory by the Bigeleisen and Mayer method.[42] Tunneling corrections were applied using a one-dimensional infinite parabolic barrier model.[43] Such KIE predictions have proven highly accurate in reactions not involving hydrogen transfer, so long as the calculation accurately depicts the mechanism and transition state geometry.[33b,34,44] The results are shown in Figure 6a.

To allow for the anharmonicity of the transition state ridge, a series of 21 equally spaced structures along the 70 cm^{-1} mode for **8-ax** were located, and the isotope effects were calculated

(40) (a) Truhlar, D. G.; Hase, W. L.; Hynes, J. T. *J. Chem. Phys.* **1983**, *87*, 2664–2682. (b) Truhlar, D. G.; Garrett, B. C.; Klippenstein, S. J. *J. Chem. Phys.* **1996**, *100*, 12771–12800.
(41) The calculations used the program QUIVER. Saunders, M.; Laidig, K. E.; Wolfsberg, M. *J. Am. Chem. Soc.* **1989**, *111*, 8989–8994. Frequencies were scaled by 0.9614. The exact choice of scaling factor makes little difference in the calculated KIE; varying the scaling factor from 0.93 to 0.97 changes the ^{13}C KIEs by less than 0.001.
(42) (a) Bigeleisen, J.; Mayer, M. G. *J. Chem. Phys.* **1947**, *15*, 261–267. (b) Wolfsberg, M. *Acc. Chem. Res.* **1972**, *5*, 225–233. (c) Bigeleisen, J. *J. Chem. Phys.* **1949**, *17*, 675–678.
(43) Bell, R. P. *The Tunnel Effect in Chemistry*; Chapman & Hall: London, 1980; pp 60–63.
(44) (a) Meyer, M. P.; DelMonte, A. J.; Singleton, D. A. *J. Am. Chem. Soc.* **1999**, *121*, 10865–10874. (b) DelMonte, A. J.; Haller, J.; Houk, K. N.; Sharpless, K. B.; Singleton, D. A.; Strassner, T.; Thomas, A. A. *J. Am. Chem. Soc.* **1997**, *119*, 9907–9908. (c) Singleton, D. A.; Merrigan, S. R.; Liu, J.; Houk, K. N. *J. Am. Chem. Soc.* **1997**, *119*, 3385–3386.

from a Boltzmann combination of all the predicted isotope effects for the 21 structures. (See the Supporting Information for details. This analysis makes assumptions regarding the separability of coordinates and the entropic equivalence of the slices, so naturally it is a rough approximation.) Because of the asymmetry of the ridge, the Boltzmann combination is weighted toward structures resembling **26**. The results are shown in Figure 6b. Both sets of predicted isotope effects match reasonably with experimental values, but the set of predicted isotope effects allowing for the asymmetry of the transition state matches slightly better.

2.7. Intermediates via "Concerted" Transition States. As discussed in the Supporting Information, a combination of calculational results and experimental observations suggest that open transition structures leading to diradical or zwitterionic intermediates are much higher in energy than the cycloaddition structures in Figure 2, so that conventional stepwise mechanisms are unlikely to play a role in these reactions. An interesting alternative, however, is that intermediates could be formed dynamically by trajectories passing through the concerted transition state. We have previously proposed that the highly asynchronous but formally concerted transition states involved in enyne—allene cyclizations can dynamically afford diradicals,[16] and Schmittel has presented strong evidence supporting this proposal.[45] In the current cases, it might be similarly envisioned that trajectories passing though the cycloaddition transition structures could lead to diradical intermediates.

To explore this idea, a short series of trajectories were again initiated starting from **8-ax** but followed now on an unrestricted (UMPW1K/6-31+G**) potential energy surface. Of 12 trajectories explored in this way, eight afforded cycloadduct in a normal way without passing through structures showing significant diradical character as gauged by the calculational total spin $\langle S^2 \rangle$. However, four of the trajectories passed into the area of the diradicaloid structure **27**, a minimum on the UMPW1K/6-31+G** surface, and did not afford **13** or **14** in up to 445 fs. This suggests the intriguing possibility that the single "concerted" cycloaddition transition structures could each lead to three species, two cycloadducts and a diradical intermediate. It should be emphasized that a standard calculational approach provides no suggestion that a diradical might be formed; the IRC leading to product **13** is spin-stable.
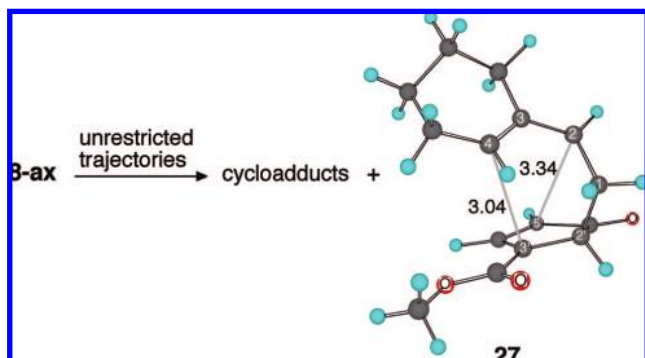

Unfortunately, the reality of **27** cannot be gauged with certainty. Structure **27** may be viewed as an analogue of the [3,3]-sigmatropic transition structure **20-ax** with greater bisallyl character. The two structures are similar and are sufficiently

Figure 7. Frontier orbital interactions between **2** and vinylcyclohexene. The size of the coefficients depicted is based on an HF/STO-3G calculation.

close in energy (the unrestricted, spin-contaminated **27** is nominally 1.7 kcal/mol below the restricted **20-ax** in PCM single-point calculations) that calculations alone cannot decide whether an intermediate is present on the surface. We note, however, that restricted calculations appear to perform better in predicting the geometry of [3,3]-sigmatropic reactions[44a] and that the restricted trajectories through **9** perform well here in predicting the observed product ratio from **5**. For this reason, the discussion here will focus on the results from the restricted trajectories.

3. Discussion

3.1. A Merging of Pathways. In applying transition state theory to the understanding of the kinetic selectivity between two products in a reaction, an assumption is made that the products arise from two distinct transition states. In the cycloadditions of **2**, the operative transition states would be envisioned as taking on separate "platonic forms" that are recognizably [$4\pi_{diene} + 2\pi_{dienone}$] or [$2\pi_{diene} + 4\pi_{dienone}$] in character. This assumption is intrinsic in qualitative theory. For example, FMO theory would attempt to account for the selectivity with **2** by examining the various possible [4 + 2] interactions and identifying the combination with the greatest overlap between the highest-energy HOMO and the lowest-energy LUMO. It is not surprising that this simple model of reactivity can fail[46] (for example this approach does not correctly predict the major product between **2** and **5**), but our emphasis here is that a basic assumption inherent in the analysis can be incorrect.

In the current reactions, the platonic [$4\pi_{diene} + 2\pi_{dienone}$] and [$2\pi_{diene} + 4\pi_{dienone}$] forms have merged at the transition state. The reason for this merging and the strong preference for the resulting transition states over alternatives can be understood from the bispericyclic idea of Caramella.[11,12] Figure 7 illustrates how the frontier orbital interactions can lead to a transition state with both [$4\pi_{diene} + 2\pi_{dienone}$] and [$2\pi_{diene} + 4\pi_{dienone}$] character. Approach of **2** to vinylcyclohexene in the *endo* orientation that would lead to product **13** maximizes HOMO—LUMO interactions. The HOMO$_{vinylcyclohexene}$—LUMO$_2$ orbital pair in Figure 7a is closer in energy than the HOMO$_2$—LUMO$_{vinylcyclohexene}$ pair of Figure 7b (8.8 eV versus 10.9 eV at HF/6-31++G(2d,p), so this orbital interaction should be more important, but both

(45) Schmittel, M.; Vavilala, C.; Jaquet, R. *Angew. Chem., Int. Ed.* **2007**, *46*, 6911–6914.

(46) (a) Kahn, S. D.; Pau, C. F.; Overman, L. E.; Hehre, W. J. *J. Am. Chem. Soc.* **1986**, *108*, 7381–7396. (b) Takasu, K.; Mizutani, S.; Ihara, M. *J. Org. Chem.* **2002**, *67*, 2881–2884. (c) Alston, P. V.; Gordon, M. D.; Ottenbrite, R. M.; Cohen, T. *J. Org. Chem.* **1983**, *48*, 5051–5054.

HOMO−LUMO pairs involve favorable [$4\pi_{\text{diene}} + 2\pi_{\text{dienone}}$] and [$2\pi_{\text{diene}} + 4\pi_{\text{dienone}}$] orbital interactions. From the size of the coefficients (HF/STO-3G), it might be expected that the [$4\pi_{\text{diene}} + 2\pi_{\text{dienone}}$] interaction would be favored by the HOMO$_{\text{vinylcyclohexene}}$−LUMO$_2$ orbital pair. but the [$2\pi_{\text{diene}} + 4\pi_{\text{dienone}}$] interaction is favored by the alternative HOMO−LUMO pair. In the transition structure **8-ax** evolving from these interactions, the [$4\pi_{\text{diene}} + 2\pi_{\text{dienone}}$] and [$2\pi_{\text{diene}} + 4\pi_{\text{dienone}}$] character is nearly equal. Only as the energy surface approaches the products is the thermodynamically more stable **13** favored.

The experimental studies of the current system support the bispericyclic nature of the transition state. The C2 KIE of ∼1.009 in the vinylcyclohexene reaction is much larger than the KIEs observed at C3 and C4 and would be extraordinarily large for a simple [$4\pi_{\text{diene}} + 2\pi_{\text{dienone}}$] cycloaddition. However, this strange observation can be qualitatively rationalized once it is understood that a bispericyclic transition state is involved, so that there is some degree of bonding to C2 at the transition state, even though this bonding does not show up in the observed product. Quantitatively, the close match between experimental and predicted ^{13}C KIEs provides support for the bispericyclic geometry of **8-ax**.

3.2. Selectivity Control Elements. 3.2.1. The Geometry of the Transition Structure. When transition state theory is applicable, the fundamentals of ground-state structural energetics are used implicitly for insight into selectivity. The central goal of the work here is to examine the qualitative ideas that must be considered to understand selectivity on bifurcating surfaces when transition state theory is not applicable. In place of transition state energetics, the guiding principles must be those of Newtonian dynamics.

In the absence of any qualitative structural considerations, the MEPs passing through each of **7** through **10** correctly predict the major product. However, even if such predictions were always correct (and they are not[47]), they offer no guidance whatsoever as to the product mixture. For example, the MEP by itself offers no reason to expect high or low selectivity from **9**, or indeed no reason to expect that **16** should be formed at all. It should also be noted that the MEP, the steepest-descent path in mass-weighted coordinates, is far from rigorously correct physically. The dynamic relevance of the steepest-descent path is the fundamental idea underlying the common use of such paths in computational chemistry, but a steepest-descent step only matches correct Newtonian dynamics when the step is arbitrarily short and starts from a resting position.

A very qualitative but intuitively more informative prediction of the selectivity can be made from the detailed geometries of the transition structures. When the C4−C3′ distance is shorter than the C2−C5′ distance, as in **7** and **8-ax**, the major product from trajectories is the [$4\pi_{\text{diene}} + 2\pi_{\text{dienone}}$] product. When the C2−C5′ distance is shorter than the C4−C3′ distance, as in **9** and **10**, the major product from trajectories is the [$2\pi_{\text{diene}} + 4\pi_{\text{dienone}}$] product. In each case, the shorter distance corresponds to the bond most likely to form. This just matches the predictions from the MEPs, but there is the added information that the difference in distance appears related to the relative selectivity. Structure **7** has a greater difference between its C4−C3′ and C2−C5′ distances than does **8-ax**, and **7** shows greater selectivity in trajectory studies. The same is true for **10** versus **9**. The

closer the geometry of the transition structure is to the platonic form intuitively expected for one of the competing pathways, the higher the selectivity.

One way of understanding why the geometry of the transition structure is a predictor of the dynamic selectivity is to consider that the geometry is related to the steepness of the paths to the products. The transition structure geometries themselves reflect to some degree the relative stabilities of the products, so one must consider the two effects together. Structure **7**, for example, is geometrically closer to **11** than it is to **12**, and there is a 22.6 kcal/mol greater drop in energy going to **11** than **12**. Combining these observations, the energy surface between **7** and **11** must be much steeper overall than the surface between **7** and **12**. For comparison, **8-ax** is geometrically more finely balanced between **13** and **14**, and the stabilities of **13** and **14** are closer than those of **11** and **12**. As a result, there is less difference between the steepness of the energy surfaces between **8-ax** and **13** versus between **8-ax** and **14**, and the selectivity is lower with **8-ax** than with **7**.

Consideration of the transition structure geometry by itself fails to rationalize aspects of the selectivity. For example, **7** and **9** have similar differences in their C4−C3′ versus C2−C5′ distances, yet trajectories passing through **7** are highly selective and those passing through **9** are nearly unselective. Understanding this observation requires consideration of another selectivity control element.

3.2.2. The Energy Surface Beyond the Transition State. The shape of the complex energy hypersurface after the cycloaddition transition state can be discerned in part from the relative energies of the cycloaddition versus Cope-rearrangement transition structures, from the geometry of the Cope transition structure, and from the relative stability of the [$4\pi_{\text{diene}} + 2\pi_{\text{dienone}}$] versus [$2\pi_{\text{diene}} + 4\pi_{\text{dienone}}$] cycloadducts. The latter factors are not independent, as the Cope transition structure follows Hammond's postulate and more closely resembles the less-stable product. This trend is opposite that seen in the cycloaddition transition structures. The contrasting shifts in the two continua of transition structures are illustrated in the Figure 8 plots of the C4−C3′ versus C2−C5′ distances. On these graphs, **7** through **10** shift toward the upper left as **19** through **22** shift toward the lower right.

The detailed position of the Cope transition structure appears to be important on the basis of the observed behavior of trajectories. As seen in Figure 8, trajectories that pass to the upper left of **19** through **22** almost always proceed to the [$2\pi_{\text{diene}} + 4\pi_{\text{dienone}}$] product, while trajectories that pass to the lower right of **19** through **22** almost always proceed to the [$4\pi_{\text{diene}} + 2\pi_{\text{dienone}}$] product. Many trajectories never approach the Cope transition structure, but for those that do, the structure represents a dividing line on the product outcome. This is hardly surprising in retrospect− in the Cope rearrangement itself the Cope transition state is *by definition* the dividing line between trajectories that pass on to product and trajectories that return to starting material. This dividing line appears to work even when the trajectories approach the dividing line from higher energy and an orthogonal dimension.

Consideration of the geometry of the Cope transition structure appears to reconcile the high selectivity of trajectories from **7** versus the low selectivity of the trajectories from **9**, despite similar differences in their C4−C3′ versus C2−C5′ distances. In the former the Cope transition structure **19** is geometrically biased toward **12** with a difference in C4−C3′ versus C2−C5′ distances of 0.22 Å. In the latter, the geometrical bias of **21**

(47) In the ene reaction of singlet oxygen with *gem*-tetramethylethylene-*d*$_6$, the MEP leads to the product of deuterium abstraction, while the major product (experimentally and in trajectory studies) is that of protium abstraction. See refs14, 15, and 18.
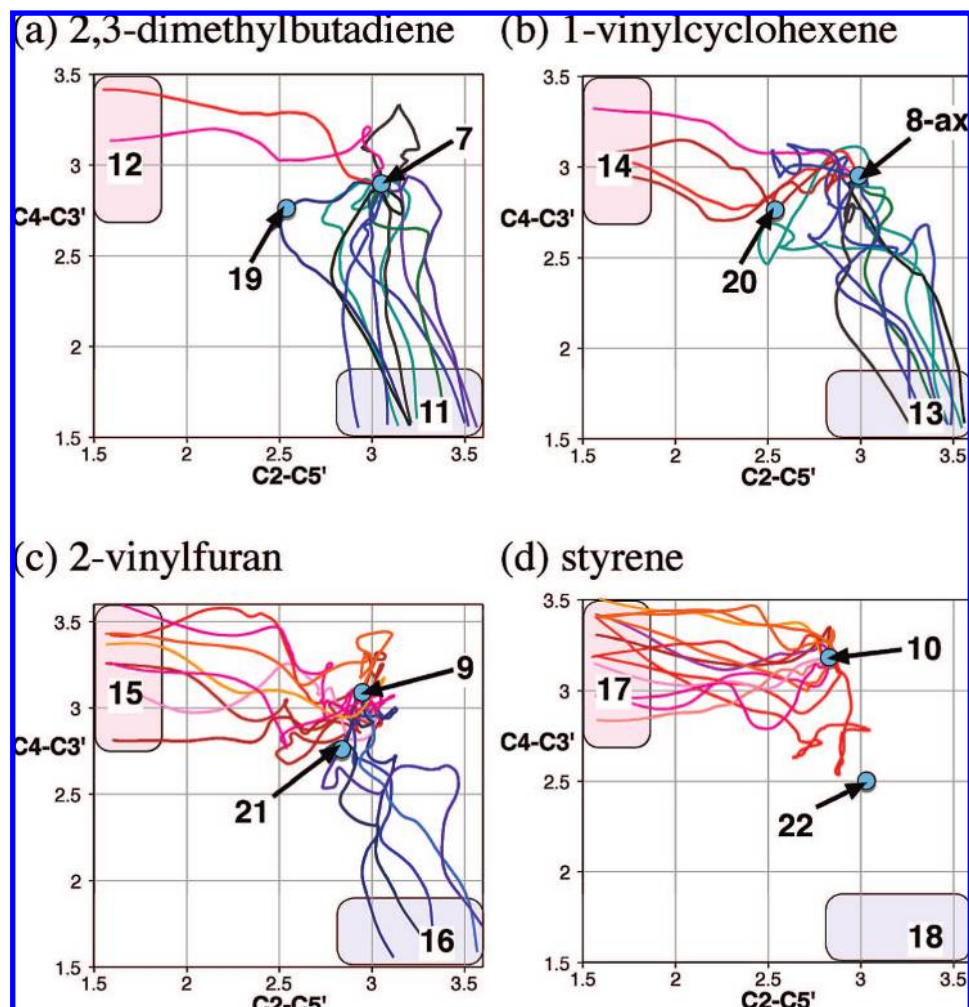
Figure 8. Plots of the C4−C3′ versus C2−C5′ distances for the various transition structures, along with plots of the C4−C3′ and C2−C5′ distance changes for sample trajectories started from (a) **7**, (b) **8-ax**, (c) **9**, and (d) **10** as they proceed toward the products.

toward **16** is smaller (in keeping with a low energy difference between **16** and **15**) with a difference in C4−C3′ versus C2−C5′ distances of only 0.08 Å. As a result, it is more likely for trajectories from **9** to pass to the "[$4\pi_{\text{diene}} + 2\pi_{\text{dienone}}$] side" of **21** than it is for trajectories from **7** to pass to the "[$2\pi_{\text{diene}} + 4\pi_{\text{dienone}}$] side" of **19**.

3.2.3. Pathways Traversing the Transition State. Trajectories cross the transition state hypersurface at a continuum of geometries with the contribution of each defined by its energy based on a Boltzmann distribution. In a three-dimensional potential energy diagram such as in Figure 5, the transition state may be viewed as a ridge to be traversed and the transition structure is the low point in the ridge. Houk has previously suggested that the passage of trajectories through the higher-energy margins of a ridge can lead to the formation of products not predicted by standard computational studies.[48]

As described in the Results section, the outcome of trajectories from **25**, **8-ax**, and **26** straightforwardly support the intuitive idea that the selectivity in reactions involving bifurcated surfaces depends on where trajectories cross the transition state ridge.

The product mixture obtained seems to vary smoothly with the position on the ridge—**25**, **8-ax**, and **26** afford 0%, 26%, and 64% of **12**, respectively. However, it should be noted that **10** and **26** are geometrically quite similar, yet trajectories from **10** are much more selective than those from **26**; this may be understood by considering the position of **20** versus **22** in Figure 8. The starting geometry makes a difference, but the energy surface beyond the transition state ridge still plays a large role in the selectivity.[46b]

A second, subtler question is whether the involvement of a range of trajectories crossing the transition state ridge makes a significant difference in the product selectivity versus that predicted solely from trajectories passing through the specific point of the transition structure. This question cannot be answered directly from the limited set of trajectories obtained here. In general terms, however, it might be expected that the transition structure will be less representative of the ensemble of trajectories crossing the transition state as the anharmonicity of the transition state ridge increases. For example, since **26** is only 0.5 kcal/mol above **8-ax** and is 0.5 kcal/mol below **25**, the trajectories passing through **26** should both contribute substantially to the product mixture and contribute by a factor of 2.3 more than the equally spaced (from **8-ax**) **25**.

With regard to the anharmonicity of the transition state ridge, the observation that allowing for the anharmonicity improves

(48) (a) Khuong, K. S.; Jones, W. H.; Pryor, W. A.; Houk, K. N. *J. Am. Chem. Soc.* **2005**, *127*, 1265–1277. (b) Because of the complexity of factors determining the selectivity, we would suggest caution in attributing the formation of unexpected materials to dynamic effects of this type in the absence of support from trajectory studies.

the prediction of the experimental KIEs is intriguing. It must be admitted that the effect is small and incompletely convincing in the current example. However, the phenomenon is reasonable and may be of greater importance to understanding experimental observations in other reactions.

3.3. Phase Space and Dynamic Matching. The control elements affecting the selectivity discussed above are all within the realm of *coordinate space*; that is, the discussion emphasized geometries and the potential energy surface, ignoring any direct effect of momenta. We discuss here briefly whether it is useful to consider control elements involving the momenta of *phase space*. Newtonian trajectories are of course deterministic, so a full consideration of phase space is a perfect predictor of selectivity. The question, however, is whether any qualitative consideration of phase-space aids in predicting or understanding selectivity. One phase-space idea considered in the literature is the role in selectivity of the excitation of particular modes,h but the most obvious candidate here is the idea of dynamic matching.[2]

Dynamic matching implies that the momentum associated with the passage through an initial transition state plays a role in subsequent selectivity. If dynamic matching is important in the selectivity here, the expectation is that there should be a relationship between the direction and magnitude of the momenta associated with the transition vectors of **7** through **10** and the product outcome. In particular, if the transition vector, i.e., the straight continuation of the path of the MEP through the saddle point, is directed toward a particular product, greater energy in the transition vector mode should be associated with selectivity toward that product.

This idea was tested by consideration of the trajectories started from **9**. The transition vector associated with **9** is aimed most closely at **15**— continuation of the transition vector from **9** decreases both the C4−C3′ and C2−C5′ distance, but the C2−C5′ distance decreases faster and the bond is formed while the C4−C3′ distance is >2.2 Å. If dynamic matching is important, it would be expected that higher energy in the transition vector would favor formation of **15**. This was not the case—the average energy in this mode for the 19 trajectories forming **15** was 170 cm^{-1} with a standard deviation of 150 cm^{-1}, while the average energy in the mode for the 12 trajectories forming **16** was 200 cm^{-1} with a standard deviation of 170 cm^{-1}. Overall, there was no statistically significant difference between the sets of trajectories, and the difference that was observed is in the wrong direction versus the expectation above. With the limited number of trajectories, it is impossible to rule out some correlation between the energy in the transition vector and the product selectivity, but the broadly overlapping range of energies for trajectories giving the two products suggests that dynamic matching is not a major factor in the selectivity here. These results also suggest that the effect of temperature on the selectivity may be low, but the temperature range applicable to the current reactions is too low to test this idea experimentally.

4. Conclusions

Dynamical theories of reaction rates and conventional transition state theory are ultimately equivalent when the assumptions of transition state theory apply,[49] but transition state theory tremendously simplifies chemistry by obviating the need to

consider the complexity of dynamics. Dynamic analyses have regained popularity in recent years, particularly in the study of enzymatic reactions, but for most reactions transition state theory is applicable and is the straightest path to understanding. The reactions here and the others discussed in the introduction constitute real exceptions to this rule. In these reactions, no simple equation predicts the selectivity. Costly trajectory studies may be applied to make a prediction of the product ratio, and the prediction based on trajectories starting from **9** is strikingly accurate (as has notably been seen in other reactions[4c,f,15,9]). However, trajectory studies provide little direct insight, certainly none at the level of transition state energetics.

The results here suggest some qualitative ideas to be considered when evaluating or predicting the selectivity for the class of dynamic effects associated with bifurcating energy surfaces. The geometry of the transition structure itself provides an initial guide to the selectivity. When the initial transition state results from the merging of two paths to products, as supported here by the calculations and the isotope effects with vinylcyclohexene, the transition structure should be somewhere in between the platonic forms expected for the individual pathways. The structure will in general more closely resemble that expected for one of the two paths, and the further from "center", the higher the selectivity. One must also consider, however, the energy surface beyond the initial transition state. A general feature of bifurcating energy surfaces is the presence of two adjacent transition states, with the second being that for the interconversion of products. The second transition state tends to act as a dividing surface for trajectories falling from the first transition state, so the position of this transition state, often predictable on qualitative grounds, affects the selectivity. A final factor for consideration is the diversity of paths taken by trajectories crossing the initial transition state. The results with trajectories starting from **25** versus **8-ax** versus **26** support the idea that the crossing point makes a difference, and consideration of the anharmonicity of the transition state ridge is likely to important in cases to understand both product mixtures and isotope effects.

All of these ideas are unsurprising in hindsight. However, it should be recognized that the control elements under discussion are outside of the conventional chemical paradigm for understanding selectivity. A growing number of reactions of this type, in which the selectivity is determined by the vagaries of dynamic trajectories, have been identified in recent years, and it is clear that the consideration of factors beyond transition state energy will often be necessary to understand the selectivity of organic reactions.

5. Experimental Section

5.1. Diels−Alder Cycloaddition of 1 and 4: Low Conversion Reaction. A mixture of 2.59 g (24 mmol) of vinylcyclohexene and 700 mg (3.2 mmol) of **1** was dissolved in 80 mL of dry THF under N$_2$ at 25 °C; then 1.33 mL (9.6 mmol) of triethylamine was added, and the reaction was left to stir overnight. An aliquot was taken before workup, and the conversion of the vinylcyclohexene as determined by ^{1}H NMR was 13%. The reaction mixture was then poured into 150 mL of saturated aqueous NaCl and extracted with 3 × 60 mL of diethyl ether. The combined organic layers were dried over MgSO$_4$ and concentrated on a rotary evaporator. The resultant oil was chromatographed on a 5 cm × 45 cm flash silica gel column using 20% ethyl acetate/hexanes as eluent to afford 625

(49) Wigner, E. *Trans. Faraday Soc.* **1938**, *34*, 29–41.

mg (79% versus **1**) of **13**. A second reaction performed by an analogous procedure was also taken to 13% conversion.

5.2. Diels−Alder Cycloaddition of 1 and 4: High Conversion Reaction. A mixture of 400 mg (3.7 mmol) of vinylcyclohexene and 300 mg (1.37 mmol) of **1** was dissolved in 38 mL of C_6D_6 under N_2 at 25 °C, and 1.6 mL (11.5 mmol) of triethylamine was added. The reaction was then heated to reflux. Aliquots were taken every 3 h and checked by ^1H NMR, and additional 300 mg portions of **1** were added until the reaction reached $99.3 \pm 0.7\%$ conversion of the vinylcyclohexene. The reaction mixture was then poured into 50 mL of saturated aqueous NaCl and extracted with 3×30 mL of diethyl ether. The combined organic layers were dried over $MgSO_4$ and concentrated on a rotary evaporator. The resultant oil was chromatographed on a 5 cm × 45 cm flash silica gel column using 20% ethyl acetate/hexanes as eluent to afford 610 mg (67% versus vinylcyclohexene) of **13**.

5.3. Diels−Alder Cycloaddition of 1 and Styrene. A mixture of 2.93 mL of styrene (25.6 mmol) and 280 mg (1.28 mmol) of **1** was dissolved in 12 mL of dry THF under N_2 at 25 °C, and 392 µL (2.8 mmol) of triethylamine was added. After stirring for 3 d at 25 °C, the reaction mixture was then poured into 120 mL of diethyl ether and washed with 50 mL of 2% $CuSO_4$ to remove triethylamine. The organic layer was washed twice with 100 mL of water, dried over $MgSO_4$ with decolorizing charcoal, and concentrated using a rotary evaporator. The resultant oil was chromatographed on a 20 mm × 250 mm flash silica gel column using hexanes as eluent to remove the styrene, followed by 5% ethyl acetate/hexanes as eluent to afford 111 mg (36%) of **17**: ^1H NMR (C_6D_6) δ 6.98 (s, 3H), 6.80 (s, 1H), 6.73 (d J = 7.0 Hz, 2H), 3.46 (s, 1H), 3.32 (s, 3H), 3.16 (m, 1H), 2.99 (m, 1H), 2.00 (m, 1H), 1.31 (m, 1H); ^{13}C NMR (CDCl$_3$) δ 201.8, 163.3, 141.8, 140.0, 137.5, 128.8, 128.1, 127.2, 56.0, 52.3, 47.9, 39.7, 30.6. HRMS: calculated $[M + Li]^+$ for $C_{15}H_{14}O_3$ 249.1103, found 249.1105.

5.4. Diels−Alder Cycloaddition of 1 and 2-Vinylfuran. A mixture of 0.82 g (8.7 mmol) of 2-vinylfuran and 400 mg (1.83 mmol) of **1** was dissolved in 30 mL of C_6D_6 under N_2 at 25 °C, and 0.75 mL (5.4 mmol) of triethylamine was added. After stirring for 2 d at 25 °C, the reaction mixture was poured into 100 mL of saturated NaCl and extracted with 3×100 mL portions of diethyl ether. The combined organic layers were washed twice with 100 mL of water, dried over $MgSO_4$, and concentrated on a rotary evaporator. The resultant oil was chromatographed on a 20 mm × 400 mm flash silica gel column

using hexanes and then 5% ethyl acetate/hexanes as eluent to afford 116 mg (27%) of **15**: ^1H NMR (C_6D_6): δ 6.89 (s, 1H), 6.80 (d J = 4.6 Hz, 1H), 5.89 (m, 1H), 5.45 (m, 1H), 3.35 (m J = 5.2 Hz, 1H), 3.27 (s, 3H), 3.13 (m, 1H), 3.01 (m, 1H), 1.84 (m J = 5.2 Hz, 1H), 1.15 (m J = 4.5, 9.6 Hz, 1H). ^{13}C NMR (C_6D_6): δ 200.0, 162.8, 155.4, 142.0, 139.8, 137.8, 110.4, 106.5, 54.0, 51.2, 47.3, 33.2, 28.5. HRMS: calculated $[M + Li]^+$ for $C_{13}H_{12}O_4$ 239.0896, found 239.0901. Two successive chromatographies afforded 80 mg (19%) of the unstable **16** in ~80% purity: ^1H NMR (C_6D_6): δ 6.91 (d J = 5.8 Hz, 1H), 6.05 (m J = 2.2, 2.7 Hz, 1H), 5.88 (d J = 5.8 Hz, 1H), 5.09 (m J = 1.2, 2.6, 2.7 Hz, 1H), 5.00 (m J = 1.2, 3.2, 3.4, 8.0 Hz, 1H), 3.60 (m J = 2.2, 2.6, 3.0, 3.2, 1H), 3.21 (s, 3H), 2.72 (m J = 2.0, 8.0, 14.9 Hz, 1H), 2.68 (m J = 2.0, 6.0 Hz, 1H), 1.71 (m J = 3.0, 3.4, 6.0, 14.9, 1H). A $^1H−^1H$ COSY spectrum of **16** exhibited cross peaks at δ (6.91, 5.88), (6.05, 5.09), (6.05, 3.60), (5.09, 5.00), (5.09, 3.60), (5.00, 3.60), (5.00, 2.72), (5.00, 1.71), (3.60, 1.71), (2.72, 2.68), (2.72, 1.71), (2.68, 1.71). HRMS: calculated $[M + Li]^+$ for $C_{13}H_{12}O_4$ 239.0896, found 239.0898.

5.5. NMR Measurements. NMR samples were prepared using 400 mg of product **13** in a 5-mm NMR tube filled to a 5-cm sample height with CDCl$_3$. The ^{13}C spectra were recorded at 125.895 MHz using inverse gated decoupling, 43.29 s delays, and an 8.493 s acquisition time to collect 512,000 points. Integrations were determined numerically using a constant equal integration region for peaks compared. A zeroth-order baseline correction is generally applied, but in no case was a first-order (tilt) correction applied. Six spectra were obtained for all three independent samples of **13**. The raw integration results are shown in the Supporting Information.

Supporting Information Available: Energies and full geometries of all calculated structures, NMR integration results for all reactions, complete reference 27a, spectra of **13**, **15**, **16**, and **17**, and the programs used for the trajectory calculations. This material is available free of charge via the Internet at http://pubs.acs.org.

JA802577V